Applications in Energy and Combustion Science 5 (2021) 100014

Contents lists available at ScienceDirect

Applications in Energy and Combustion Science

journal homepage: www.elsevier.com/locate/jaecs

Investigation of nitric oxide formation in methane, methane/propane, and methane/hydrogen flames under condensing gas boiler conditions

Jörn Hinrichs*, Maximilian Hellmuth, Felix Meyer, Stephan Kruse, Marco Plümke, Heinz Pitsch

Rheinisch-Westfalische Technische Hochschule Aachen, Aachen, Germany

ARTICLE INFO

Keywords:
Burner-stabilized flames
NO_x formation
Hydrogen combustion
Condensing gas boiler conditions
Resolved simulation
Experimental measurements

ABSTRACT

In this study, NO_x formation in lean premixed burner-stabilized flames was investigated under condensing gas boiler operating conditions for pure methane, methane/propane, and methane/hydrogen mixtures. Temperature and NO_x species profiles were experimentally obtained from thermocouple and wet chemiluminescence detector measurements using in-situ extracted gas samples. Resolved simulations utilizing different NO sub-mechanisms from the GRI 2.11, the GRI 3.0, the CRECK mechanism, and a recent mechanism from Glarborg and co-workers were performed, where the mechanism from Glarborg showed the best agreement with the measured NO_x concentrations. While the other mechanisms also agreed fairly well with the experiments, a pathway analysis revealed that this results from error compensation, where the prompt pathway was underestimated, which was balanced by an overestimated contribution of the NNH pathway. Interestingly, the prompt pathway was found to be the major NO_x formation route for condensing gas boiler conditions despite the lean mixture. While the temperature level in the post-flame region was too low for the thermal pathway to become dominant, the NNH and N_2O pathways reached their chemical equilibrium just downstream of the flame front and therefore did not further contribute to the overall NO_x emissions.

The partial substitution of methane by hydrogen slightly reduced NO_x emissions, which was similarly found in experiment and simulation. The post-flame temperature for methane/hydrogen remained nearly unchanged, because the higher adiabatic flame temperature compared to pure methane was compensated by increased heat losses due to a higher laminar burning velocity. The addition of hydrogen decreased the amount of CH radicals in the flame front, which led to a lower contribution of the most important prompt pathway.

Substituting methane by propane increased the temperature level due to a higher adiabatic flame temperature and a slightly smaller laminar burning velocity. While increasing NO_x emissions were found in the experiment, the simulation predicted a minimally smaller NO_x level compared to pure methane. The higher temperature caused increasing contributions of the thermal, NNH, and N_2O pathways. For the prompt pathway, which is again the most important NO_x formation route, the temperature trend was superimposed by a decreasing CH concentration in the flame front.

1. Introduction

The unavoidable formation of nitrogen oxides (NO_x) during the combustion of fuels with air represents a significant harm to the environment. NO_x emissions – comprising the species of nitric oxide (NO) and nitrogen dioxide (NO_2) – contribute to ozone depletion, cause the production of photochemical smog, and are dangerous to human health [1,2].

One third of the total energy consumption in Europe is required to provide domestic hot water and heating. With a share of roughly 80 %, natural gas represents the main energy source [3]. Consequently, household gas burners significantly contribute to global NO_x emissions and legal regulations like the European norm DIN EN 15502 were established, which stipulate NO_x emission limits for new gas-fired boilers [4,5].

Several studies analyzed the combustion characteristics and emission formation in condensing gas boiler systems from a global perspective [6–8]. Hinrichs et al. [9] provided detailed information on local CO and NO_x formation in the heating unit of a condensing gas boiler. Experimental measurements of radial temperature, CO, and NO profiles revealed significant inhomogeneities in the combustion chamber depending on the considered axial height. This complicated the comparison with resolved simulations of a representative burner hole. However, well validated temperature and NO_x species profiles are a prerequisite to analyze the contribution of the various NO formation pathways in more detail.

* Corresponding author.
E-mail address: j.hinrichs@itv.rwth-aachen.de (J. Hinrichs).

https://doi.org/10.1016/j.jaecs.2020.100014
Received 20 July 2020; Received in revised form 9 November 2020; Accepted 9 November 2020
Available online 13 November 2020

In order to increase the reliability of the simulation and identify suitable measures to reduce NO_x emissions from condensing gas boilers, further analyzes on NO_x formation in laminar premixed flames were performed in the present study on a simplified perforated-plate burner. The burner setup was derived from the cylindrical multi-hole burner considered in Ref. [9], but set up in a way to provide well-defined boundary conditions for the simulation.

Many studies have already dealt with NO formation in premixed flames on perforated-plate burners. Konnov et al. [10–13] and Coppens et al. [14,15] studied NO formation in adiabatic flames for various fuels numerically and experimentally applying the the heat flux method proposed by de Goey et al. [16].

Glarborg et al. [2] pointed out in their recent review article that even though NO formation was subject of extensive research over the last decades, the governing chemical processes are still not fully understood. Consequently, many studies developed or improved detailed reaction mechanisms for NO formation in recent decades [2,10–15,17–28].

In a step towards evaluating existing NO mechanisms, Kovacs et al. [29] collected a huge amount of data including various experimental setups and operating conditions from more than 30 publications and compared 17 existing NO mechanisms with experimental data. They found that the mechanism from Glarborg et al. [2] showed the overall best agreement for this large data set. However, Kovacs et al. [29] only focused on N/H/O elementary reactions and neglected hydrocarbon fuels like methane, ethane, or propane, which are major components in natural gas commonly used in condensing gas boilers. Therefore, the question remains if the mechanism from Glarborg et al. [2] is also able to capture NO_x formation in condensing gas boilers using common natural gas components. The NO_x prediction capabilities of the NO submechanism from Glarborg et al. [2] were compared to different well-known NO reaction mechanisms under condensing gas boiler conditions and validated with experimental measurements in this study.

The emerging role of advanced fuels from renewable resources, such as hydrogen, and local fluctuations in the gas quality enforce a high fuel-flexibility of novel condensing gas boilers, while ensuring safe and stable burner operation and simultaneously meeting emission regulations. The European norm DIN EN 437 [30] defines several test gas compositions, for which emission norms need to be fulfilled. Therefore, pure methane, methane/hydrogen, and methane/propane flames were studied and their impact on the NO_x formation was investigated.

The effect of substituting methane by hydrogen or propane on NO_x formation has already been studied in literature [14,20,31–34]. Boyd Fackler et al. [34] experimentally studied NO formation in a jet-stirred reactor at atmospheric conditions and found a modest increase in NO with increasing C/H ratio, while hydrogen led to a lower NO level. Williams et al. [33] analyzed CH and NO concentrations in premixed pure methane and propane flames under low-pressure conditions. They found higher NO concentrations in propane flames under lean conditions than for pure methane, even though the CH concentration in propane flames was lower and the prompt pathway was by far the most important pathway. They concluded that other intermediate carbon species significantly contribute to the NO formation, which were not considered by the used NO reaction mechanisms. Pillier et al. [20] also investigated laminar premixed flames of methane and methane/propane numerically and experimentally under low-pressure conditions. They concluded that NO remains unchanged when methane is partially substituted by ethane or propane (<10 %) for a given equivalence ratio. Bohon et al. [35,36] investigated various alkanes and renewable alcohols in Bunsen-type flames and in a McKenna burner. They found slightly increased NO_x emissions for lean propane-air- compared to methane-air-mixtures for both burner configurations [36].

It is challenging to transfer the findings of different fuel types and burner configurations on NO_x formation from literature to the applied case of condensing gas boilers. The usage of different fuels affects the adiabatic flame temperature and radical concentrations, which are important influencing variables for NO_x formation. In addition, the laminar burning velocity varies for different fuels leading to different stand-off distances and flame heat losses to the burner. This impacts the post-flame temperature and may dominate the other influencing factors. Therefore, the complex interaction of the different fuel types on NO_x formation were investigated using a generic perforated-plate burner in the present study.

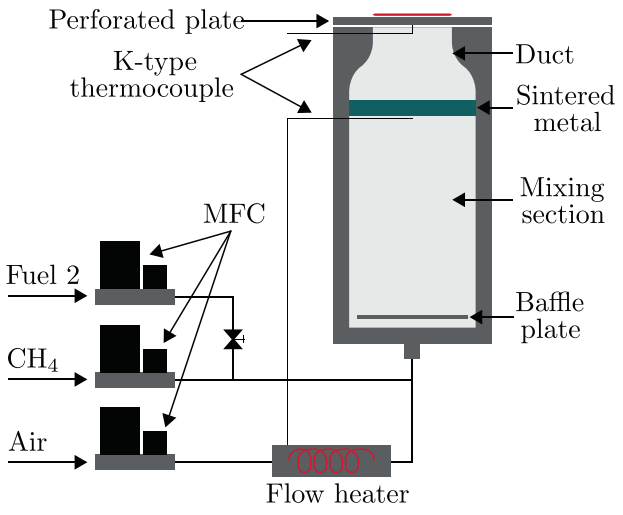

Fig. 1. Schematic illustration of the perforated-plate burner test bench.

2. Experimental methods

2.1. Burner setup

The investigated perforated-plate burner was derived from the cylindrical multi-hole burner contained in the condensing gas boiler device studied previously [9]. The surface of the perforated-plate burner was scaled down by a factor of 7.84 compared to the multi-hole burner. The mass flows were decreased by the same factor to obtain identical outflow velocities and an equal load per area. In the full system, a laminar outflow in the burner holes was observed even for nominal loads of 25.8 kW [9]. Scaling the burner dimensions is therefore not disturbed by turbulent structures. Consequently, the resulting flow field above the perforated-plate burner is laminar, too.

The original multi-hole burner had a locally different hole pattern with burner hole diameters of 0.6 mm and 1.0 mm, a spatially varying porosity, and a complex internal flow field induced by a swirler. To enable a better comparison of resolved simulation and experiment, the perforated-plate burner was designed to obtain a homogeneous flame structure with well-defined boundary conditions. The perforated plate has a homogeneous, hexagonally arranged hole pattern with a constant hole diameter of 1.0 mm. The porosity of the plate matches the global porosity of the original multi-hole burner and amounts to 0.31. Diameter and thickness of the perforated plate are 50.0 mm and 1.0 mm, respectively.

The burner test bench, which is schematically illustrated in Fig. 1, consisted of an insulated steel cylinder with the perforated plate mounted at the outlet. Fuel and oxidizer streams were adjusted by mass flow controllers (MFC) and premixed upstream of the burner inlet. The uncertainty of the MFCs amounts to 0.2% of the maximum and 0.8% of the current mass flow. A flow heater in the oxidizer line allowed to control the unburnt temperature of the premixed gas. A mixing device consisting of a baffle plate and a mixing section ensured a homogeneous fuel/oxidizer mixture at the burner exit. Behind the mixing device, a sintered metal plate eliminated velocity inhomogeneities of the gas flow. To minimize boundary layer effects at the wall, a contoured duct was

used. The temperature of the unburnt premixed gas was measured with two K-type thermocouples, one below the perforated plate and one below the sintered metal. The edge of the perforated plate was wrapped up with insulating material to minimize heat losses to the steel cylinder.

All experiments were carried out at a fixed load point of 0.77 kW, which refers to a load point of the original condensing gas boiler with high NO_x emissions. Three different fuel mixtures, which represent different types of natural gas according to the European norm DIN EN 437 [30], were studied: G20 (100% methane), G21 (87% methane and 13% propane), and G222 (77% methane and 23% hydrogen).

The oxidizer was air and the equivalence ratio was set to $\Phi = 0.8$ for all fuel-air mixtures. The unburnt gas temperature was set to 313 K to account for preheating effects of the condensing gas boiler. All measurements were conducted at atmospheric pressure.

2.2. Temperature and NO_x measurements

An Al_2O_3-coated fine gauge bare wire R-type thermocouple from OMEGA with a bead diameter of 0.6 mm was employed for gas temperature measurements. The manufacturer specifies the measurement error below ± 2.5 K. The thermocouple is mounted in a constant-tension thermocouple configuration [37]. In hot environments, particularly radiative heat losses bias thermocouple measurements. Hence, a correction routine based on the approach of Shaddix [38] was applied. Details of this procedure can be found in the supplemental material Appendix A.1.

To measure local NO_x concentrations, a deactivated stainless steel tubing (1.5875 mm x 1.0 mm ID) was utilized for gas sampling. Since stainless steel is thermally more stable than quartz glass, a smaller probe could be used. This increased the accessibility and the spatial resolution of the measurement compared to common quartz glass probes. It was noted by England et al. [39] that catalytic reduction reactions of NO with unburnt hydrocarbons and CO can occur in stainless steel probes for nearly-stoichiometric to fuel-rich mixtures. Therefore, the NO_x measurements in the flame front might be affected, because noteworthy amounts of CO and other hydrocarbon species are present. The results in the post-flame region are not affected though due to the lean conditions used.

The sampling probe was connected to a wet chemiluminescence detector (NGA2000 WCLD manufactured by Rosemount) for analysis. The analyzer was calibrated with a reference gas mixture consisting of 90 ppm NO in N_2. The measurement error is specified by the manufacturer as 1% for the measurement range of 100 ppm, which results in an error of ± 1 ppm.

The thermocouple and sampling probe were consecutively mounted on the skid of a linear guide unit, which allowed automatic vertical displacement above the perforated plate. The relative spatial uncertainty is specified by the manufacturer (Rose + Krieger) to 0.5%. Measurements were performed ranging from the burner surface (0 mm) to 14 mm above the burner. For each height above the burner, data was recorded with 10 measurements per second over a period of 20 s, resulting in 200 measurements per position. Three measurement sequences were performed for each condition to acquire a reliable dataset. The profiles shown for temperature and NO_x concentration are based on the mean values of the three measurement sequences.

The solid temperature of the perforated plate was recorded using a K-type thermocouple from OMEGA with an outer diameter of 0.25 mm and a measurement accuracy of ± 2.5 K. The thermocouple was inserted from downstream into a blind hole in the center of the plate with a diameter of 0.3 mm and depth of 0.5 mm. To bond the thermocouple to the plate, a high temperature ceramic adhesive from OMEGA was applied.

3. Numerical framework

In order to gain a deeper understanding of NO_x formation, resolved simulations including finite rate chemistry were performed. For this, the in-house simulation code CIAO of the Institute for Combustion Technology was used [40]. The details of the numerical framework are described in Ref. [9].

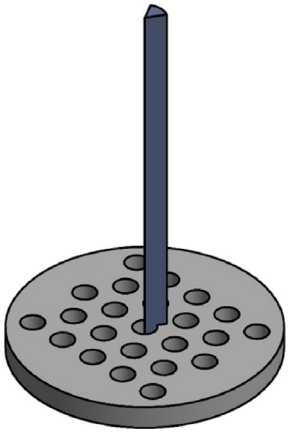

Fig. 2. Schematic diagram of the perforated plate with hexagonal hole pattern. Blue surfaces represent the 2D simulation domain, which is rotationally symmetric to the center of the hole.

The perforated-plate burner was designed to obtain spatially uniform laminar inflow and plate temperature profiles resulting in a homogeneous premixed flame. This along with the symmetry of the perforated plate was used to isolate a small hexagonal unit cell. According to Goswami et al. [41], it is reasonable to approximate this unit cell by an axisymmetrical cell of a single burner hole. The 2D simulation domain is rotationally periodic with the axis of rotation passing through the center of the burner hole. A schematic diagram of the perforated plate and the resulting simulation domain are illustrated in Fig. 2.

The simulation domain starts just upstream of the perforated plate and ends 15 mm above. A velocity inlet and an outflow boundary condition were applied. The radial dimension amounts to 0.895 mm to capture the porosity of the perforated plate. Slip and no-flux boundary conditions were prescribed at the round edge of the domain. The surface of the burner plate was defined as no-slip wall with a Dirichlet boundary condition for the plate temperature.

In order to resolve the velocity field within the burner hole, 2D cold flow simulations have been performed beforehand and a radial grid resolution of 30 cells in the area of the burner hole was derived. The grid resolution around the flame front was estimated prior to the resolved simulations by 1D simulations of unstretched premixed flames using FlameMaster [42–44]. The area of the flame in axial direction was resolved with 60 cells along the flame front to accurately capture temperature and species gradients. The resulting numerical grid consisted of 49,050 cells. The smallest cell size used in the numerical grid was 5.8 µm and the corresponding time step size amounted to 2.3 µs.

Simulations for three fuel mixtures of G20, G21, and G222 were performed at atmospheric pressure using an equivalence ratio of $\Phi = 0.8$ and an inlet gas temperature of T_u = 313 K. The inlet velocities were specified from the experimental mass flow rates. The perforated plate temperatures were derived from the experimental measurements and are summarized together with the other boundary conditions in Table 1. In addition, laminar burning velocities and adiabatic flame temperatures for all fuel mixtures have been evaluated from 1D simulations of unstretched premixed flames using FlameMaster. These flame characteristics support the evaluation of stand-off distances, flame heat losses, and burnt gas temperatures and are also listed in Table 1.

To represent the laminar burner-stabilized flame within the simulation, the Navier-Stokes equations in cylindrical formulation were solved in the low-Mach number limit as described by Desjardins et al. [40]. Within the species transport equations, diffusivity was derived from the unity Lewis number assumption for all species except for hydro-

Table 1
Boundary conditions and flame characteristics for the fuel mixtures G20, G21, and G222.

	G20	G21	G222
Mole fraction CH_4	100%	87%	77%
Mole fraction C_3H_8	0%	13%	0%
Mole fraction H_2	0%	0%	23%
Inlet velocity	0.1607 m/s	0.1573 m/s	0.1611 m/s
Plate temperature	728 K	732 K	765 K
Laminar burning velocity	0.274 m/s	0.271 m/s	0.311 m/s
Adiabatic flame temperature	2010 K	2023 K	2017 K

gen. For hydrogen, a constant non-unity Lewis number was utilized ($Le_{H_2} = 0.269$ and $Le_H = 0.161$), which was evaluated in the burnt gas region of a 1D unstretched premixed flame simulation [45]. The assumption of unity Lewis numbers for all species except for hydrogen was verified by simulations of unstretched premixed flames, which resulted in the same temperature and species concentration profiles as if all Lewis numbers were set to constant non-unity values. Species diffusion due to temperature gradients (Soret effect), thermal conduction due to species gradients (Dufour effect) as well as heating due to viscous dissipation were neglected. In contrast to the condensing gas boiler, the perforated-plate burner represents an open system, where radiation effects are important. Therefore, radiation heat losses were considered by the optically thin gas (OTG) model.

Most reaction mechanisms in literature focusing on the formation of nitric oxides also contain species and reactions for the combustion of hydrocarbon fuels. NO_x formation cannot be considered separately from the hydrocarbon part of the mechanism, because the latter determines the radical concentrations and temperature level of the flame. As NO is extremely sensitive to these quantities, an unbiased comparison of different NO sub-mechanisms is only possible, when the identical mechanism for the hydrocarbon combustion serves as a basis. Usually, there is a one-way coupling between NO formation and hydrocarbon oxidation reactions, i.e. the fuel oxidation affects the NO formation, but inversely NO formation has only a marginal impact on the main hydrocarbon oxidation process. This allows to couple different NO sub-mechanisms with one hydrocarbon mechanism as a basis.

In the current study, the hydrocarbon part of the mechanism from Blanquart et al. [46] is used as reference and coupled with different NO sub-mechanisms. The mechanism from Blanquart et al. [46] contains 149 species and 1651 reactions and was initially designed for engine-relevant fuels. The oxidation of smaller alkanes is derived from the well validated GRI 3.0 mechanism [47], where only a few rates have been updated according to recent findings [45,46]. Recently, a reduced version of this mechanism was applied to lean, premixed methane-air flames in several studies [9,45], where the mechanism showed good agreement with measured temperature and CO mole fraction data. The formation of the methylidyne radical (CH), which initiates NO formation via the prompt pathway, is included in the hydrocarbon mechanism and is therefore identical for all flames and NO sub-mechanisms.

Originally, the mechanism from Blanquart et al. [46] included the NO sub-mechanism of the GRI 2.11 with 9 species and 73 reactions [48]. Besides, the NO sub-mechanism of the GRI 3.0 [47] with 17 species and 212 reactions is considered in the current study. Compared to the more recent mechanisms discussed next, these might be outdated, but they have been used in several recent studies focusing on NO_x formation [9,25,29,34,45,49]. The GRI mechanisms are well-known and often serve as a reference for more recent mechanisms.

To examine the development in the understanding of NO formation processes, the NO sub-mechanisms of the GRI 2.11 and GRI 3.0 are compared to more recent NO sub-mechanisms like the CRECK mechanism by Faravelli et al. [18] and Frassoldati et al. [19,22], and the very recent mechanism by Glarborg et al. [2]. The CRECK mechanism contains 30 species and 260 reactions and is applicable to low and high temperature ranges [18,19]. Later, it was extended to capture the NO formation in hydrogen-air flames [22]. Glarborg et al. [2] published a very comprehensive review article on the four different NO formation pathways. Their focus was on revising rate coefficients and activation energies based on existing experimental data and theoretical work. The revised NO sub-mechanism is the most detailed one considered in the present study and includes 82 species and 1528 reactions. The details of the NO sub-mechanisms used are summarized in Table 2.

Besides these NO sub-mechanisms, plenty of other mechanisms focusing on NO formation have been published [10–13,21,23–26]. Lamoureux et al. [25] developed an NO sub-mechanism named NOmecha2.0, which was coupled to the hydrocarbon mechanism of the GDFKin3.0 from El Bakali et al. [21]. Another mechanism on NO formation was published by Shrestha et al. [26], who extended the NOmecha2.0 mechanism for NO_x formation in ammonia-air flames. The hydrocarbon mechanism as well as NO_x chemistry has been validated for freely propagating and burner-stabilized premixed flames, shock-tube, jet-stirred reactor, and plug-flow reactor experiments [26]. However, both mechanisms have only been validated for premixed methane-air flames at low pressures, which does not match the conditions considered in this study.

4. Results and discussion

4.1. Methane flame validation

To study the four different NO sub-mechanisms, the simulation results along the centerline f or pure methane (G20) are compared to the experimentally measured data. In Fig. 3a, it can be seen that all simulation results exhibit exactly the same temperature profile, which is caused by the identical hydrocarbon mechanism used as a basis for the different NO sub-mechanisms. In addition, all non-nitrogen radical profiles are identical for the four simulations, which proves that NO_x formation does not influence the fuel oxidation for condensing gas boiler operating conditions. This enables an unbiased comparison of the different NO sub-mechanisms, which is not affected by varying temperatures or radical concentrations. The profiles of the most important radicals initiating NO_x formation (O, OH, H, and CH) are illustrated in Fig. A.9 in the supporting material in Appendix A.

Until a height above burner (HAB) of 1.0 mm, the experimental temperature is higher than in the simulation. This was already found previously and explained by large temperature gradients in radial direction, which could not be resolved by the experiment due to the dimensions of the thermocouple bead [9]. Moreover, thermocouple measurements represent an invasive technique affecting the flame and flow field especially close to the burner surface. At 1.0 mm HAB, the experimental temperature profile shows a characteristic peak, which is not visible in the simulated profiles. The origin for this peak is assumed to also result from the invasive measurement technique. The thermocouple is strongly glowing when it is inserted into the hot region. The radiation of the thermocouple bead preheats the cold unburnt mixture leaving the burner hole of the perforated plate, which increases the enthalpy level of the flame. This measurement artifact is amplified by the plate itself, since its surface partially reflects the radiation. The effect quickly vanishes when the thermocouple is moved further away from the perforated plate, because the radiation of the thermocouple bead spreads spherically to a larger area and the local preheating effect reduces simultaneously. This effect was also visible in the measured temperature profiles of Bohon et al. [36], who did thermocouple along with OH LIF thermometry measurements. The same characteristic peak is also visible for the other fuel mixtures G21 and G222.

In the post-flame region, the simulated temperature level is located above the experimental profile. However, in light of the uncertainties of the temperature measurements due to radiation correction, simulation and experiment show reasonably good agreement. At 3.0 mm HAB, the simulated temperature lies 53.8 K or 2.94% above the experimental

Table 2
Details of the NO sub-mechanisms used in the present study.

	GRI 2.11 [48]	**GRI 3.0** [47]	**CRECK** [18,19,22]	**Glarborg** [2]
Species	9	17	30	82
Reactions	73	212	260	1528

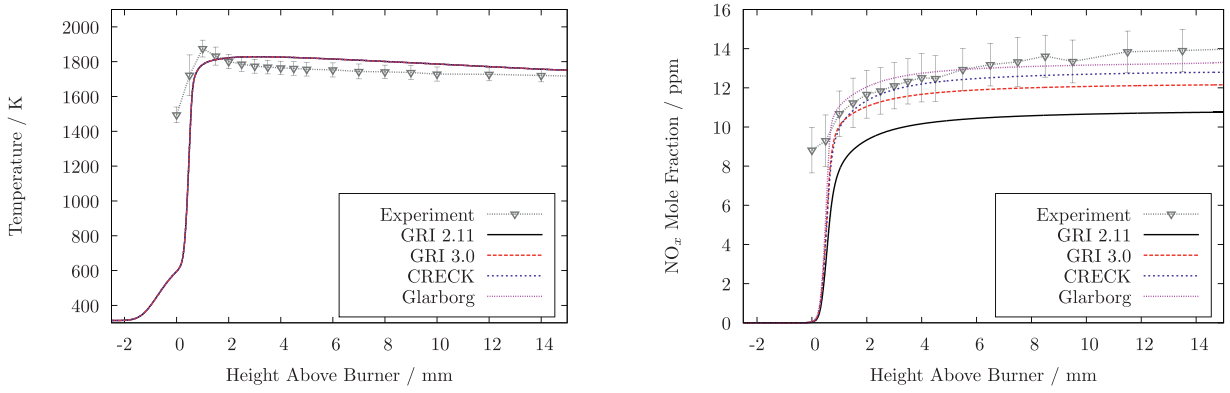

(a) Temperature (b) NO_x

Fig. 3. Centerline profiles of temperature and NO_x mole fraction of four NO sub-mechanisms along with the experimental data for pure methane (G20).

measured level. In addition, the slope of the temperature profile in the post-flame region due to gas radiation effects and the predicted stand-off distance match well between simulation and experiment.

In Fig. 3b, the simulated NO_x mole fraction profiles of the four mechanisms along the centerline are displayed together with the experimentally measured data. At the burner surface, the experiment determines a NO_x concentration of 8.82 ppm, while the simulation does not predict any NO_x, because the gas is still unburnt at that position. Similar to the thermocouple measurements, probe sampling measurements represent an invasive technique, which impacts flame front and flow field close to the burner. Moreover, large gradients in radial direction cannot be resolved due to the dimensions of the gas sampling probe. The same behavior is found for the fuel mixtures G21 and G222.

All simulations capture the experimental trend that NO_x is only formed within and closely downstream of the flame front from 0.5 mm to 3.0 mm HAB. The NO sub-mechanism from Glarborg shows the best agreement with the experiment with a NO_x mole fraction of 13.28 ppm at 14.0 mm HAB compared to 13.91 ppm of the experiment. This is closely followed by the CRECK mechanism, which reaches a final NO_x mole fraction of 12.76 ppm. The predicted NO_x levels of the GRI 3.0 and GRI 2.11 mechanisms are further below the experimental values with 12.13 ppm and 10.73 ppm, respectively.

However, considering the uncertainties of the measurements, the radiation correction, and the usage of only one hydrocarbon mechanism, it is difficult to evaluate which NO sub-mechanism captures NO_x formation in condensing gas boilers best by just regarding the total NO_x profiles. Lamoureux et al. [25] investigated the impact of their experimental temperature uncertainty of 4 % on NO_x formation and found a 30 % increase of NO_x. Therefore, a more detailed analysis on NO_x formation pathways was done for all NO sub-mechanisms.

4.2. Analysis of NO_x formation pathways

To gain a deeper understanding how the thermal, prompt, NNH, and N_2O pathways contribute to the total NO_x concentration, a pathway analysis according to Trisjono et al. [45] is performed. Details of the procedure are outlined in the supporting material Appendix A.3.

In Fig. 4, the contributions of these four pathways are integrated along the domain and correlated to the total NO_x formation. While

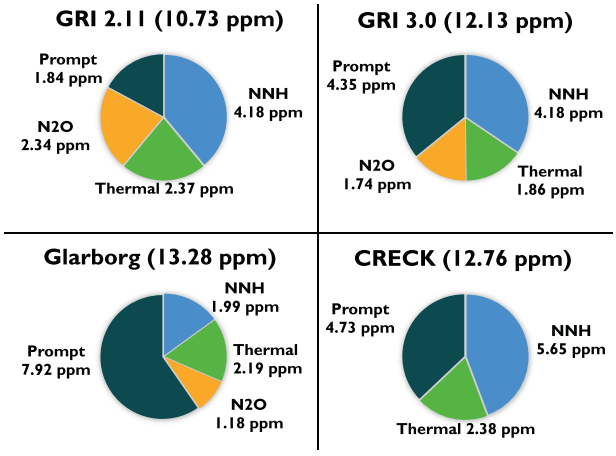

Fig. 4. Integrated NO_x mole fractions produced via the prompt, thermal, NNH, and N_2O pathways of four NO sub-mechanisms for pure methane (G20).

the total NO_x concentration for the different NO sub-mechanisms only varies by 2.6 ppm or 19.5 %, the integrated contributions for the different pathways differ significantly.

The Glarborg NO sub-mechanism predicts the largest contribution by the prompt pathway with 59.6 %, which is much larger than the 17.1% to 37 % determined by the other mechanisms.

For the GRI 2.11, GRI 3.0 and CRECK NO sub-mechanisms, the NNH pathway is a major NO_x formation route with shares ranging from 35.4 % to 44.3 %. In contrast to this, the NNH pathway only plays a minor role in the Glarborg NO sub-mechanism with a contribution of 15 %.

Regarding the remaining NO_x formation pathways, only small fractions of NO_x are formed via the thermal pathway, which are roughly similar for all NO sub-mechanisms. The contributions of the N_2O pathway vary from 0 % to 21.8 % for the different NO sub-mechanisms.

To further analyze the cause for these significantly varying contributions between the different NO sub-mechanisms, net production rate profiles of each pathway for all mechanisms are shown in Fig. 5.

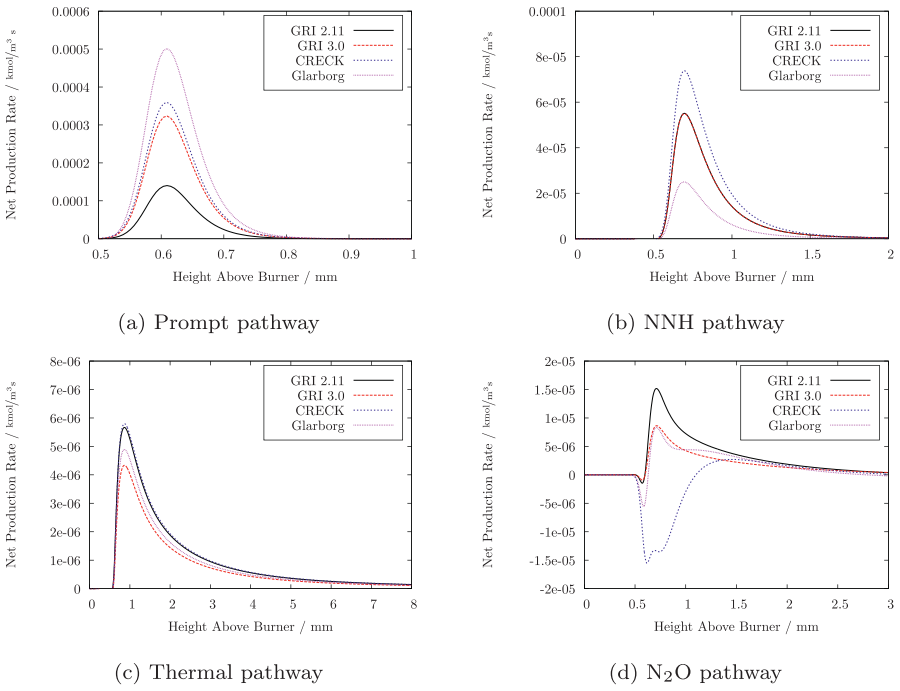

(a) Prompt pathway (b) NNH pathway

(c) Thermal pathway (d) N_2O pathway

Fig. 5. Net production rates of the prompt, NNH, thermal, and N_2O pathways of four NO sub-mechanisms for pure methane (G20).

As can be seen in Fig. 5a, the prompt pathway is only active within the flame, since it requires CH or CH_2 radicals, which cannot be found in the post-flame region for lean premixed conditions. Comparing the different NO sub-mechanisms, a clear chronological trend of increasing prompt formation rates is visible. The oldest NO sub-mechanism of the GRI 2.11 predicts a net formation rate, which is more than three times smaller than the one determined by the most recent mechanism of Glarborg et al. [2]. The GRI 2.11 only considers $N_2 + CH \rightleftharpoons HCN + N$ as initiating reaction of the prompt pathway, which was postulated by Fenimore [50]. The GRI 3.0 and the CRECK mechanisms also consider this reaction, even though ab-initio molecular orbital calculations have shown that this reaction does not conserve the electron spin [51]. Instead, the reaction $N_2 + CH \rightleftharpoons NCN + H$ was proposed by Moskaleva and Lin [52], which is used in the Glarborg NO sub-mechanism. The corresponding reaction rate coefficients used by Glarborg et al. [2] are much larger than those used in the other NO sub-mechanisms. This follows a recent study from Klippenstein et al. [53], who reanalyzed the reaction rates of important prompt NO reactions. Except for the GRI 2.11, all mechanisms contain further reactions belonging to the prompt pathway, e.g. $N_2 + CH \rightleftharpoons HNCN$, but these reactions play a minor role under condensing gas boiler operating conditions.

In Fig. 5b, the net formation rates of the NNH pathway are displayed. Closely behind the flame front, this pathway reaches its chemical equilibrium and therefore does not further contribute to the total NO_x formation. The initiation reaction $N_2 + H \rightleftharpoons NNH$ produces significant amounts of NNH. However, most of the NNH produced is directly reburned via $NNH + O_2 \rightleftharpoons N_2 + HO_2$. Only small amounts of NNH finally form NO via $NNH + O \rightleftharpoons NO + NH$. The small net formation rates of the NNH pathway determined by the Glarborg NO sub-mechanism refer to studies from Haworth et al. [54] and Klippenstein et al. [55], who noted that the importance of the NNH pathway was severely overestimated in previous mechanisms.

These recent findings on NO_x formation via the NNH and prompt pathway reveal some kind of error compensation for the GRI and CRECK mechanisms, where the overestimated contributions of the NNH pathway are balanced by underestimated formation rates of the prompt pathway.

The thermal pathway, which is displayed in Fig. 5c, is the simplest NO formation pathway. All NO sub-mechanisms consider $N_2 + O \rightleftharpoons NO + N$ as the only initiating reaction and the corresponding net formation rates vary by less than 50 % between the different mechanisms. The thermal pathway is the only pathway contributing to NO_x formation in the post-flame region. However, the temperature level is rather low due to the lean mixture, flame heat losses to the perforated plate and due to gas radiation, which decreases the production of thermal NO_x to almost insignificant levels.

The profiles of the N_2O pathway in Fig. 5d exhibit negative and positive net production rates in the flame front for the Glarborg and the two GRI mechanisms. The initiating reaction $N_2 + O \rightleftharpoons N_2O$, which competes with the thermal pathway, produces by far the largest amount of N_2O compared to the other initiating reactions. While significant parts of the N_2O produced are reburned via $N_2O + H \rightleftharpoons N_2 + OH$, only a small fraction is converted to NO via $N_2O + H \rightleftharpoons NO + NH$. In the post-flame region, the N_2O pathway reaches its chemical equilibrium. The profile of the CRECK NO sub-mechanism significantly differs from all other mechanisms, because only negative net formation rates are found within the flame front. Here, N_2O is formed via $NNH + O \rightleftharpoons N_2O + H$, which is then reburned to N_2. This explains the negative net formation rates and the zero contribution of the N_2O pathway to the total NO_x emissions predicted by the CRECK mechanism. While this reaction channel is not considered in the GRI mechanisms, its importance is much smaller in the Glarborg mechanism than in the CRECK mechanism. The strong interaction between the N_2O and NNH pathway was also discussed by Bohon et al. [36].

Concluding the comparison of the four NO sub-mechanisms studied, the agreement with the experimental data is acceptable for all mechanisms, taking the uncertainties of the measurements, the radiation correction, and the hydrocarbon mechanism into account. However, the detailed pathway analysis revealed error compensation effects for the GRI 2.11, GRI 3.0, and CRECK mechanisms, where the contribution of the NNH pathway was overestimated and the NO_x formation via the prompt pathway was underestimated. Only the NO sub-mechanism from Glarborg et al. [2], which also showed the best agreement with the measured NO_x concentration profile, did not show this behavior and is there-

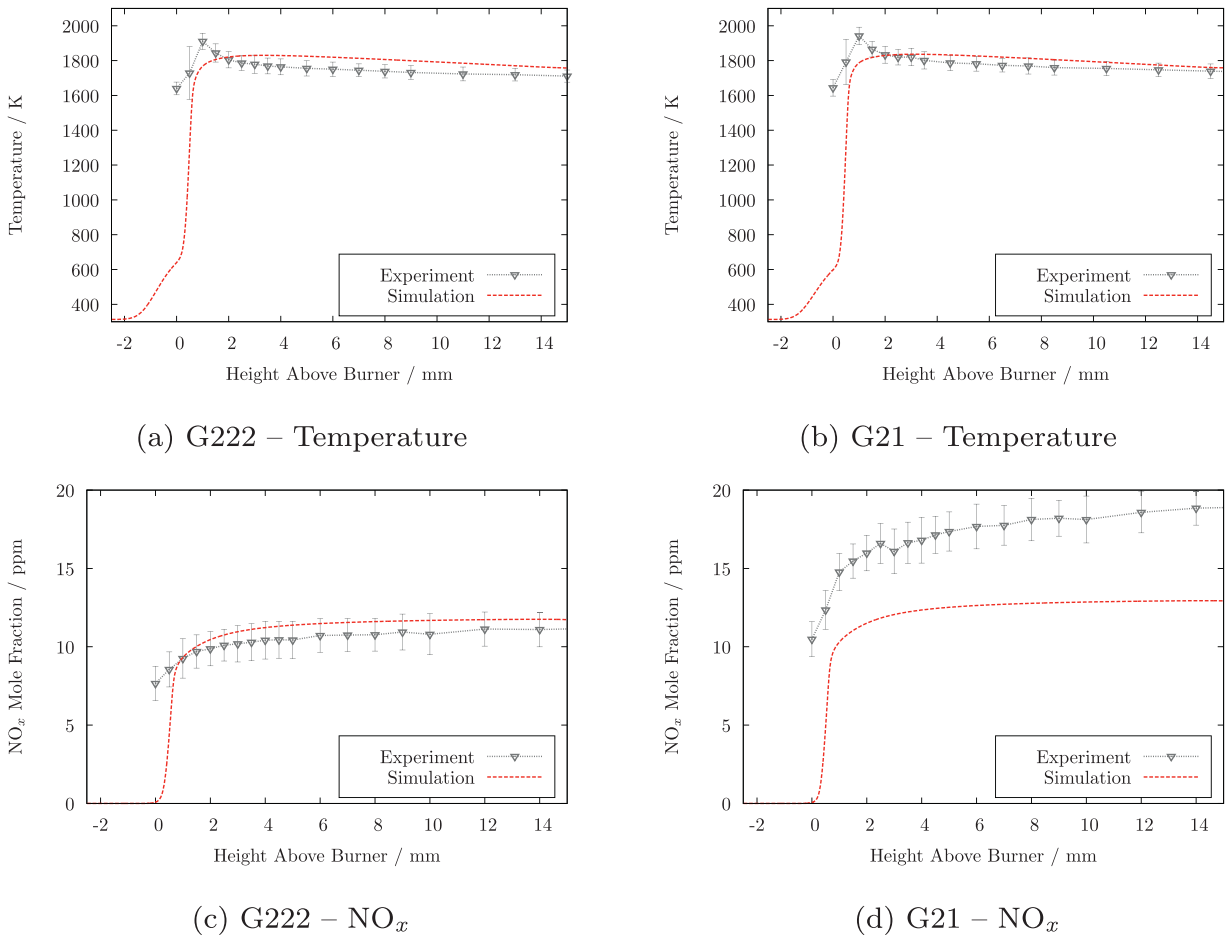

Fig. 6. Centerline profiles of temperature and NO_x mole fraction of simulation and experiment for methane-hydrogen (G222) and methane-propane (G21) mixtures.

fore the best of the studied NO sub-mechanisms for the application in condensing gas boiler conditions.

4.3. Effect of hydrogen and propane addition on NO_x formation

To study the effect of partially substituting methane by hydrogen or propane on NO_x formation, the fuel mixtures G222 (77 % methane and 23 % hydrogen as molar fractions) and G21 (87 % methane and 13 % propane as molar fractions) are compared to the reference fuel G20 (100 % methane). As the previous section identified the NO sub-mechanism from Glarborg et al. [2] to represent NO_x formation under condensing gas boilers best, this mechanism was also used for the G222 and G21 flames.

Computed and measured temperature profiles of the G222 and G21 flames in Fig. 6a and b show good agreement. The simulated temperature of G222 deviates by 50.5 K or 2.8 % from the experiment at 3.0 mm HAB. For G21, the difference amounts to 15.8 K or 0.86 % at the same axial position.

The addition of hydrogen increases the adiabatic flame temperature compared to pure methane as listed in Table 1. However, the post-flame temperature remains nearly unchanged in comparison with G20. This is caused by higher flame heat losses to the burner due to an also increasing laminar burning velocity. This conclusion is supported by the experimental measurement of the perforated plate temperature. For G222, a plate temperature of 765 K was recorded compared to a plate temperature of 728 K for G20, which was shown in Table 1.

The substitution of methane by propane leads to a higher adiabatic flame temperature compared to pure methane as illustrated in Table 1. While a higher flame temperature would increase the flame heat losses to the burner, the slightly smaller laminar burning velocity of G21 compensates this effect. This is supported by the measured plate temperature of 732 K for G21, which is only 4 K higher than for G20.

In Fig. 6c and d, the NO_x mole fraction profiles of G222 and G21 are displayed. For G222, NO_x is only formed within and just behind the flame front, which is correctly represented by the simulation. The profiles of simulation and experiment match reasonably well with NO_x mole fractions of 11.74 ppm and 11.10 ppm at 14.0 mm HAB. This represents a relative deviation of 5.45 %.

For G21, the simulation underestimates the NO_x level found in the experiment by 31.83 % with 12.85 ppm compared to 18.85 ppm at 14.0 mm HAB. The experiment detects a small but steady rise of the NO_x profile in the post-flame region. This is not visible in the simulated NO_x profile, even though the simulation slightly overpredicts the temperature level in the post-flame region. One explanation for the deviating NO_x formation might be the radical concentration in the flame front and post-flame zone resulting from the hydrocarbon mechanism. This was also suggested by Bohon et al. [36], who studied lean premixed propane-air flames and found noteworthy deviations between simulation and experiment. The hydrocarbon mechanism of Blanquart et al. [46] was not specifically validated to capture the flame characteristics of propane, which might affect the results of the G21 flame. To further study the deviation of the NO_x concentration for G21 and gain a deeper insight into the effect of the fuel composition on the individual NO_x formation routes, a pathway analysis is performed.

In Fig. 7, the integrated NO_x mole fractions resulting from the prompt, thermal, NNH, and N_2O pathways are illustrated for G20, G21, and G222. The contributions of the NNH, thermal, and N_2O pathways vary only slightly for the three fuel mixtures. Only the prompt pathway,

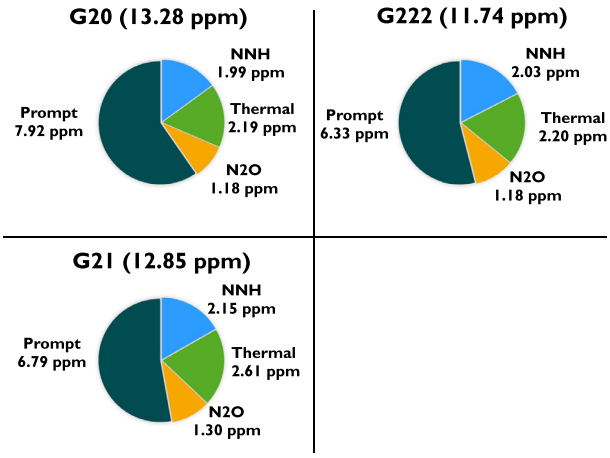

Fig. 7. Integrated NO_x mole fractions produced via the prompt, thermal, NNH, and N_2O pathways for G20, G21, and G222.

which is most important for all fuel mixtures, shows significant differences depending on the fuel mixture. G20 exhibits the highest contribution from the prompt pathway with 7.92 ppm. For G222, the determined contribution of the prompt pathway is 1.59 ppm lower than for G20, even though the temperature level is nearly the same. G21 shows the highest temperature level, but it exhibits a lower integrated NO_x mole fraction with 6.79 ppm than for G20. It can be concluded that the temperature level is not the most important driving factor of the prompt pathway.

Therefore, the CH mole fraction profile is analyzed in Fig. 8, which represents the most important radical to initiate the consumption of nitrogen via this pathway. G222 shows the lowest CH concentration in the flame front, which is caused by a lower amount of carbon atoms in the fuel mixture. G20 shows the highest CH concentration of all fuel mixtures, which explains the overall largest contribution of the prompt pathway to the total NO_x emissions. Finally, G21 shows a lower CH concentration than G20 despite the higher amount of carbon atoms in the fuel mixture, which justifies the lower contribution of the prompt pathway. This agrees with findings from Bakali et al. [21], who noted that substituting methane by propane decreases the CH concentration in the flame.

5. Summary and conclusion

Modern condensing gas boilers exhibit relatively low temperature levels, which significantly reduces the importance of the thermal pathway to the total NO_x emissions. Instead, other formation routes become more important. Moreover, a high fuel-flexibility is necessitated from novel condensing gas boilers to take into account the emerging role of advanced fuels from renewable resources, such as hydrogen. These topics have been addressed in the current study by performing detailed numerical and experimental analyses of NO_x formation in premixed burner-stabilized flames under condensing gas boiler conditions using a generic perforated-plate burner.

The GRI 2.11 [48] and the GRI 3.0 [47] mechanisms, which have been developed some time ago, but have been used in several recent studies on NO_x formation [9,25,29,34,45,49], were compared to more recent, detailed NO sub-mechanisms from the CRECK mechanism [18,19,22] and the mechanism from Glarborg et al. [2]. The Glarborg NO sub-mechanism showed the best agreement with the experimental NO_x data for pure methane (G20), but also the other mechanisms agreed fairly well. However, a detailed pathway analysis revealed error compensation effects for the GRI and CRECK mechanisms, where the contribution of the NNH pathway was overestimated, which was then balanced by too small prompt formation rates. Consequently, the Glarborg mechanism turned out to be the best mechanism of the ones studied to capture NO_x in condensing gas boiler applications.

As expected, the thermal pathway exhibited a small contribution to the total NO_x concentration. The NNH and N_2O pathways quickly reached their chemical equilibrium behind the flame front, which limited their contribution to the NO_x emissions. The prompt pathway, which is only active within the flame front under condensing gas boiler conditions, turned out to be the major NO_x formation route.

The effect of partially substituting methane by hydrogen increases the adiabatic flame temperature. However, the post-flame temperature of the methane/hydrogen mixture (G222) remains nearly unchanged compared to pure methane. This is caused by higher flame heat losses due to an also increased laminar burning velocity. The resulting NO_x emissions of G222 are lower than for G20 as predicted by simulation and experiment. This originates from lower CH concentrations in the flame front, which mainly influence the NO_x formation rate of the most important prompt pathway.

The partial substitution of methane by propane leads to an increased post-flame temperature due to a higher adiabatic flame temperature and a slightly smaller laminar burning velocity. While the tempera-

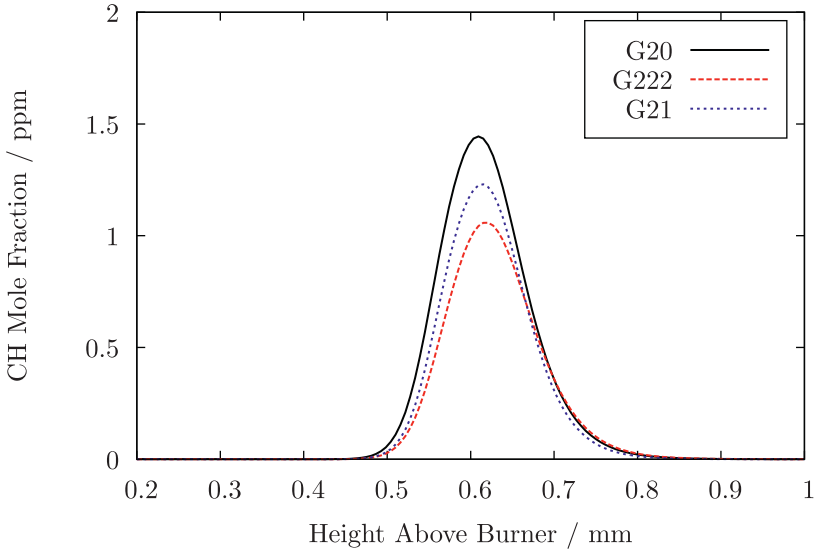

Fig. 8. Centerline profiles of CH mole fraction for G20, G21, and G222.

ture profile is predicted very well by the simulation, the NO_x level of methane/propane (G21) is underestimated in comparison with the experiment. A pathway analysis identified the prompt pathway as the major NO_x formation route. For G21, the CH concentration was found to be lower than for G20 despite a higher carbon content.

The major relevance of the prompt pathway to NO_x formation has to be taken into account in future efforts to reduce NO_x emissions of condensing gas boilers. Besides, the sensitivity of the prompt pathway to the CH concentration in the flame front highlights the requirement towards the hydrocarbon mechanism. As discussed by Pillier et al. [20], Williams et al. [33], and Glarborg et al. [2], important CH formation reactions exhibit large uncertainties. This necessitates a further validation of the hydrocarbon mechanism used to represent lean premixed burner-stabilized flames under condensing gas boiler conditions.

Acknowledgements

The authors from RWTH Aachen University gratefully acknowledge funding from Vaillant GmbH.

Declaration of Competing Interest

The authors declare that they have no known competing financial interests or personal relationships that could have appeared to influence the work reported in this paper.

Supplementary material

Supplementary material associated with this article can be found, in the online version, at 10.1016/j.jaecs.2020.100014

References

[1] Badr O, Probert S. Oxides of nitrogen in the earth's atmosphere: trends, sources, sinks and environmental impacts. Appl Energy 1993;46(1):1–67. doi:10.1016/0306-2619(93)90076-2.
[2] Glarborg P, Miller JA, Ruscic B, Klippenstein SJ. Modeling nitrogen chemistry in combustion. Prog Energy Combust Sci 2018;67:31–68. doi:10.1016/j.pecs.2018.01.002.
[3] der Deutschen Heizungsindustrie (BDH) B. Effiziente Systeme und erneuerbare Energien. Tech. Rep.; 2017. Frankfurter Str. 720 - 726, 51145 Cologne, Germany
[4] Gas-fired heating boilers - Part 1: General requirements and tests, German version EN15502-1:2012. 2012a.
[5] Gas-fired central heating boilers - Part 2-1: Specific standard for type C appliances and type B2, B3 and B5 appliances of a nominal heat input not exceeding 1 000 kW; German version EN 15502-2-1:2012. 2012b.
[6] Lee S, Kim J-M, Kum S-M, Lee C-E. Suggestion on the simultaneous reduction method of CO and NOx in premixed flames for a compact heat exchanger. Energy Fuels 2010;24(2):821–7. doi:10.1021/ef9008554.
[7] Lee S, Kum S-M, Lee C-E. An experimental study of a cylindrical multi-hole premixed burner for the development of a condensing gas boiler. Energy 2011;36(7):4150–7. doi:10.1016/j.energy.2011.04.029.
[8] Lee PH, Hwang SS. Formation of lean premixed surface flame using porous baffle plate and flame holder. J Therm Sci Technol 2013;8(1):178–89. doi:10.1299/jtst.8.178.
[9] Hinrichs J, Felsmann D, Bortoli SS-D, Tomczak H-J, Pitsch H. Numerical and experimental investigation of pollutant formation and emissions in a full-scale cylindrical heating unit of a condensing gas boiler. Appl Energy 2018;229:977–89. doi:10.1016/j.apenergy.2018.08.011.
[10] Konnov AA, Dyakov IV, Ruyck JD. Probe sampling measurements and modeling of nitric oxide formation in methane-air flames. Combust Sci Technol 2001;169(1):127–53. doi:10.1080/00102200108907843.
[11] Konnov AA, Dyakov IV, de Ruyck J. Nitric oxide formation in premixed flames of $H_2 + CO + CO_2$ and air. Proc Combust Inst 2002;29(2):2171–7. doi:10.1016/S1540-7489(02)80264-4.
[12] Konnov A, Dyakov I. Nitrous oxide conversion in laminar premixed flames of $CH_2 + O_2 + Ar$. Proc Combust Inst 2009;32(1):319–26. doi:10.1016/j.proci.2008.07.020.
[13] Konnov AA, Dyakov IV, Knyazkov DA, Korobeinichev OP. Formation and destruction of nitric oxide in NO doped premixed flames of C_2H_4, C_2H_6, and C_3H_8 at atmospheric pressure. Energy Fuels 2010;24(9):4833–40. doi:10.1021/ef100527s.
[14] Coppens F, Ruyck JD, Konnov A. The effects of composition on burning velocity and nitric oxide formation in laminar premixed flames of $CH_4 + H_2 + O_2 + N_2$. Combust Flame 2007;149(4):409–17. doi:10.1016/j.combustflame.2007.02.004.
[15] Coppens F, Ruyck JD, Konnov A. Effects of hydrogen enrichment on adiabatic burning velocity and NO formation in methane + air flames. Experimental Thermal and Fluid Science 2007;31(5):437–44. doi:10.1016/j.expthermflusci.2006.04.012. Fourth Mediterranean Combustion Symposium
[16] de Goey LPH, van Maaren A, Quax RM. Stabilization of adiabatic premixed laminar flames on a flat flame burner. Combust Sci Technol 1993;92(1–3):201–7. doi:10.1080/00102209308907668.
[17] Luque J, Smith GP, Crosley DR. Quantitative CH determinations in low-pressure flames. Symp (Int) Combust 1996;26(1):959–66. doi:10.1016/S0082-0784(96)80308-0.
[18] Faravelli T, Frassoldati A, Ranzi E. Kinetic modeling of the interactions between NO and hydrocarbons in the oxidation of hydrocarbons at low temperatures. Combust Flame 2003;132(1):188–207. doi:10.1016/S0010-2180(02)00437-6.
[19] Frassoldati A, Faravelli T, Ranzi E. Kinetic modeling of the interactions between NO and hydrocarbons at high temperature. Combust Flame 2003;135(1):97–112. doi:10.1016/S0010-2180(03)00152-4.
[20] Pillier L, Bakali AE, Mercier X, Rida A, Pauwels J-F, Desgroux P. Influence of C_2 and C_3 compounds of natural gas on NO formation: an experimental study based on LIF/CRDS coupling. Proc Combust Inst 2005;30(1):1183–91. doi:10.1016/j.proci.2004.08.057.
[21] Bakali AE, Pillier L, Desgroux P, Lefort B, Gasnot L, Pauwels J, et al. NO prediction in natural gas flames using GDF-Kin 3.0 mechanism NCN and HCN contribution to prompt-NO formation. Fuel 2006;85(7):896–909. doi:10.1016/j.fuel.2005.10.012.
[22] Frassoldati A, Faravelli T, Ranzi E. A wide range modeling study of NOx formation and nitrogen chemistry in hydrogen combustion. Int J Hydrogen Energy 2006;31(15):2310–28. doi:10.1016/j.ijhydene.2006.02.014.
[23] Konnov A. Implementation of the NCN pathway of prompt-NO formation in the detailed reaction mechanism. Combust Flame 2009;156(11):2093–105. doi:10.1016/j.combustflame.2009.03.016.
[24] Goos E, Sickfeld C, Mauss F, Seidel L, Ruscic B, Burcat A, et al. Prompt NO formation in flames: the influence of NCN thermochemistry. Proc Combust Inst 2013;34(1):657–66. doi:10.1016/j.proci.2012.06.128.
[25] Lamoureux N, Merhubi HE, Pillier L, de Persis S, Desgroux P. Modeling of NO formation in low pressure premixed flames. Combust Flame 2016;163:557–75. doi:10.1016/j.combustflame.2015.11.007.
[26] Shrestha KP, Seidel L, Zeuch T, Mauss F. Detailed kinetic mechanism for the oxidation of ammonia including the formation and reduction of nitrogen oxides. Energy Fuels 2018;32(10):10202–17. doi:10.1021/acs.energyfuels.8b01056.
[27] Shrestha KP, Eckart S, Elbaz AM, Giri BR, Fritsche C, Seidel L, et al. A comprehensive kinetic model for dimethyl ether and dimethoxymethane oxidation and NOx interaction utilizing experimental laminar flame speed measurements at elevated pressure and temperature. Combust Flame 2020;218:57–74. doi:10.1016/j.combustflame.2020.04.016.
[28] de Persis S, Pillier L, Idir M, Molet J, Lamoureux N, Desgroux P. NO formation in high pressure premixed flames: experimental results and validation of a new revised reaction mechanism. Fuel 2020;260:116331. doi:10.1016/j.fuel.2019.116331.
[29] Kovacs M, Papp M, Zsely IG, Turanyi T. Determination of rate parameters of key N/H/O elementary reactions based on $H_2/O_2/NOx$ combustion experiments. Fuel 2020;264:116720. doi:10.1016/j.fuel.2019.116720.
[30] Prüfgase – Prüfdrücke – Gerätekategorien; Deutsche Fassung EN 437:2018. 2018.
[31] Steele RC, Jarrett AC, Malte PC, Tonouchi JH, Nicol DG. Variables affecting NOx formation in lean-premixed combustion. Turbo Expo 1995;3. doi:10.1115/95-GT-107.
[32] Turbiez A, Bakali AE, Pauwels J, Rida A, Meunier P. Experimental study of a low pressure stoichiometric premixed methane, methane/ethane, methane/ethane/propane and synthetic natural gas flames. Fuel 2004;83(7):933–41. doi:10.1016/j.fuel.2003.10.017.
[33] Williams BA, Fleming JW. Experimental and modeling study of NO formation in 10torr methane and propane flames: Evidence for additional prompt-NO precursors. Proc Combust Inst 2007;31(1):1109–17. doi:10.1016/j.proci.2006.07.246.
[34] Boyd Fackler K, Karalus M, Novosselov I, Kramlich J, Malte P, Vijlee S. NOx behavior for lean-premixed combustion of alternative gaseous fuels. J Eng Gas Turb Power 2016;138(4):041504. doi:10.1115/1.4031478.
[35] Bohon MD, Guiberti TF, Mani Sarathy S, Roberts WL. Variations in non-thermal NO formation pathways in alcohol flames. Proc Combust Inst 2017;36(3):3995–4002. doi:10.1016/j.proci.2016.05.024.
[36] Bohon MD, Guiberti TF, Roberts WL. PLIF measurements of non-thermal NO concentrations in alcohol and alkane premixed flames. Combust Flame 2018;194:363–75. doi:10.1016/j.combustflame.2018.05.024.
[37] Cundy VA, Morse JS, Senser DW. Constant-tension thermocouple rake suitable for use in flame mode combustion studies. Rev Sci Instrum 1986;57(6):1209–10. doi:10.1063/1.1138631.
[38] Shaddix CR. Correcting thermocouple measurements for radiation loss: a critical review. Tech. Rep.. Sandia National Labs, Livermore, CA (US); 1999.
[39] England C, Houseman J, Teixeira D. Sampling nitric oxide from combustion gases. Combust Flame 1973;20(3):439–42. doi:10.1016/0010-2180(73)90035-7.
[40] Desjardins O, Blanquart G, Balarac G, Pitsch H. High order conservative finite difference scheme for variable density low mach number turbulent flows. J Comput Phys 2008;227(15):7125–59. doi:10.1016/j.jcp.2008.03.027.
[41] Goswami M, Coumans K, Bastiaans RJM, Konnov AA, de Goey LPH. Numerical simulations of flat laminar premixed methane-air flames at elevated pressure. Combust Sci Technol 2014;186(10–11):1447–59. doi:10.1080/00102202.2014.934619.
[42] Cai L, Minwegen H, Beeckmann J, Burke U, Tripathi R, Ramalingam A, et al. Experimental and numerical study of a novel biofuel: 2-butyltetrahydrofuran. Combust Flame 2017;178:257–67. doi:10.1016/j.combustflame.2016.12.021.
[43] Cai L, Minwegen H, Kruse S, Daniel Buettgen R, Hesse R, Ramalingam A, et al. Exploring the combustion chemistry of a novel lignocellulose-derived biofuel: cyclopentanol. Part II: experiment, model validation, and functional group analysis. Combust Flame 2019;210:134–44. doi:10.1016/j.combustflame.2019.08.025.

[44] Langer R, Lotz J, Cai L, vom Lehn F, Leppkes K, Naumann U, et al. Adjoint sensitivity analysis of kinetic, thermochemical, and transport data of nitrogen and ammonia chemistry. Proc Combust Inst 2020. doi:10.1016/j.proci.2020.07.020.
[45] Trisjono P, Pitsch H. A direct numerical simulation study on NO formation in lean premixed flames. Proc Combust Inst 2017;36(2):2033–43. doi:10.1016/j.proci.2016.06.130.
[46] Blanquart G, Pepiot-Desjardins P, Pitsch H. Chemical mechanism for high temperature combustion of engine relevant fuels with emphasis on soot precursors. Combust Flame 2009;156(3):588–607. doi:10.1016/j.combustflame.2008.12.007.
[47] Smith G.P., Golden D.M., Frenklach M., Moriarty N.W., Eiteneer B., Goldenberg M., Hanson R.K., Song S., Gardiner Jr. W.C., Lissianski V.V., Qin Z., http://www.me.berkeley.edu/gri_mech/; 1995
[48] Bowman C.T., Hanson R.K., Davidson D.F., et al., GRI-Mech 2.11, 1995, http://www.me.berkeley.edu/gri_mech/.
[49] Pillier L, Idir M, Molet J, Matynia A, de Persis S. Experimental study and modelling of NOx formation in high pressure counter-flow premixed CH_4/air flames. Fuel 2015;150:394–407. doi:10.1016/j.fuel.2015.01.099.
[50] Fenimore C. Formation of nitric oxide in premixed hydrocarbon flames. Symp (Int) Combust 1971;13(1):373–80. doi:10.1016/S0082-0784(71)80040-1.
[51] Cui Q, Morokuma K, Bowman J, Klippenstein S. The spin-forbidden reaction CH(2II) + N_2=HCN + N(4S) revisited. II. Nonadiabatic transition state theory and application. J Chem Phys 1999;110(19):9469–82. doi:10.1063/1.478949.
[52] Moskaleva L, Lin M. The spin-conserved reaction CH + N_2=H + NCN: a major pathway to prompt NO studied by quantum/statistical theory calculations and kinetic modeling of rate constant. Proc Combust Inst 2000;28(2):2393–401. doi:10.1016/S0082-0784(00)80652-9.
[53] Klippenstein SJ, Pfeifle M, Jasper AW, Glarborg P. Theory and modeling of relevance to prompt-NO formation at high pressure. Combust Flame 2018;195:3–17. doi:10.1016/j.combustflame.2018.04.029.
[54] Haworth NL, Mackie JC, Bacskay GB. An ab initio quantum chemical and kinetic study of the NNH + O reaction potential energy surface: how important is this route to NO in combustion? J Phys Chem A 2003;107(35):6792–803. doi:10.1021/jp034421p.
[55] Klippenstein SJ, Harding LB, Glarborg P, Miller JA. The role of NNH in NO formation and control. Combustion and Flame 2011;158(4):774–89. doi:10.1016/j.combustflame.2010.12.013. Special Issue on Kinetics